BL9127880

PUBLICAÇÕES

IFUSP/P-891

INVERSION POTENTIAL FOR THE $\alpha+{}^{12}C$ SYSTEM

R. Lichtenthäler Filho, A.C.C. Villari, A. Lépine-Szily
and L.C. Gomes
Instituto de Física, Universidade de São Paulo

Fevereiro/1991

INVERSION POTENTIAL FOR THE α + ^{12}C SYSTEM

R. Lichtenthäler Fº, A.C.C. Villari, A. Lépine-Szily and L.C. Gomes
Departamento de Física Nuclear - Instituto de Física da U.S.P.
Caixa Postal 20516 - 01498 São Paulo, SP - Brasil

ABSTRACT

The α + ^{12}C elastic scattering angular distributions at E_{LAB} = 120 MeV, 145 MeV and 172,5 MeV were phase-shift analized and an inversion procedure for the determination of the optical potential was applied. The potential and its associated uncertainties, as a function of the radial distance, were found. Comparison is made with usual Wood-Saxon optical potential analysis.

1. INTRODUCTION

The problem of determining the potential from the S-matrix elements for fixed energy is extensively discussed in the literature[1] and some approximate methods have been developed and applied to nuclear physics problems. For example, Lipperheid and Fiedeldey[2] based their method on the assumption that if S_ℓ is a simple rational function of ℓ, a simple method can be applied for the determination of V(r). Another approach is the semi-classical extension of Kujawski[3] to complex potentials. A further different approach is proposed by Cooper, Ioannides and Mackintosh[4,5] based on an iterative-pertubative procedure.

For the purpose of investigating the uncertainties in the optical potential resulting from the errors associated to the experimental measurements of elastic cross section we found the method of reference (4) most convenient. Thus we adopt their procedure and use the measurements of S. Wiktor et al.[8]: for the $\alpha + {}^{12}C$ system at E_{LAB} = 120 MeV, 145 MeV and 172,5 Mev as our input data. Our choice of this set of data, apart from its good quality was based on the fact that at the energies measured we expect the $\alpha + {}^{12}C$ system to be reasonably transparent to allow a sufficiently precise determination of the optical potential. In section 2 we describe and illustrate the inversion procedure. Section 3 contains a description of our analysis and in section 4 we draw our major conclusions.

2. THE INVERSION PROCEDURE

We assume that the elastic scattering matrix S_ℓ is reproduced by the spherically symmetric optical potentital V(r) for two colliding spinless nuclei. If $\overset{\bullet}{V}(r)$ is an approximation to V(r) and $\overset{\bullet}{S}_\ell$ its corresponding scattering matrix the following relation is easily obtained:

$$S_\ell - \overset{\bullet}{S}_\ell = - \frac{4\mu i}{\hbar^2 k} \int_0^\infty \chi_\ell(r)\overset{\circ}{\chi}_\ell(r)\left[V(r)-\overset{\bullet}{V}(r)\right]dr \tag{2.1}$$

where μ is the reduced mass of the system and k the wave number for the elastic channel. $\chi_\ell(r)$ and $\overset{\circ}{\chi}_\ell(r)$ are the radial wave function amplitudes for the angular momentum $\hbar\ell$ corresponding to V(r) and $\overset{\bullet}{V}(r)$ respectively. We have imposed the following normalization at infinity:

$$\chi_\ell(r) \underset{r \to \infty}{=} \frac{1}{2}\left[G_\ell - iF_\ell - S_\ell\ (G_\ell + iF_\ell)\right]$$

and similarly for $\overset{\circ}{\chi}_\ell(r)$. F_ℓ and G_ℓ are the regular and irregular

Coulomb wave functions as defined by Abramowitz and Segun[7]. Eq. (2.1) is the starting point for the inversion procedure.

We set

$$\chi_\ell(r) = \overset{0}{\chi}_\ell(r)$$

in Eq. (2.1) which transforms it into a linear integral equation for the dimensionless function f(r):

$$f(r) = \left[V(r) - \overset{\bullet}{V}(r) \right] / E_0$$

where E_0 is the kinetic energy of the ions in the elastic channel.

We assume that the nuclear potential contributes to S_ℓ only for $\ell < \ell_{max}$. Next we choose a basis of N linearly independent functions $y_i(r)$ to represent f(r) in the interval (0, r_{max}). For r_{max} we may take the classical closest approach radius for the ions in the presence of the Coulomb field with angular momentum $\hbar\ell_{max}$. For $y_i(r)$ we used the linear splines as we found this most convenient.

With these arrangments Eq. (2.1) transforms into a set of algebraic linear equations.

$$S_\ell - \overset{0}{S}_\ell \equiv \delta S_\ell = \sum_{i=1}^{N} B_{\ell i} a_i \qquad 0 \le \ell \le \ell_{max} \tag{2.2}$$

with $$f(r) = \sum_{i=1}^{N} a_i \; y_i(r)$$

and $$B_{\ell i} = -2ik \int_0^\infty \left[\overset{0}{\chi}_\ell(r) \right]^2 y_i(r) dr \tag{2.4}$$

The coefficients a_i are determined by taking $N<\left[\ell_{max}+1\right]$ and minimizing the expression:

$$\chi^2 = \frac{1}{\ell_{max}+1-N}\sum_{\ell=0}^{\ell_{max}}\left|\delta S_\ell - \sum_{i=1}^{N} B_{\ell i}a_i\right|^2 W_\ell \qquad (2.5)$$

where W_ℓ are weighting factors. We have taken

$$W_\ell = (2\ell+1)/(\ell_{max}+1).$$

The procedure can now be summarized: (i) we choose $\hat{V}(r)$ as a starting potential; (ii) we fix ℓ_{max}, r_{max} and the linear spline basis that cover the interval $(0, r_{max})$; (iii) we determine a_i by requiring χ^2 to be minimum; (iv) we find a new potential $\hat{V}(r) + E_0 f(r)$ and (v) we repeat the above procedure starting with the new potential until convergence is reached.

Figure I exibts an example that illustrates the procedure. We took as target S_ℓ those generated by the Wood-Saxon optical potential of reference (6).

$$V(r) = \frac{V_0}{1+\exp\left[\frac{r-R}{a}\right]} + i\,\frac{W_0}{1+\exp\left[\frac{r-R}{a_i}\right]}\ ;\ R = r_0\left[A_P^{1/3} + A_T^{1/3}\right]$$

where the parameters are given in the second column of table I.

For the starting potential we also used a Wood-Saxon shape for the real part with parameters given in the third column of table I with the imaginary part set to be zero. We chose ℓ_{max} = 40 and r_{max} = 10fm and used a basis of 20 linear splines equally spaced over the interval (0,10fm). The procedure converged after seven iterations with final χ^2 = 0,00096. After each iteration we calculate the distance between the target S_ℓ and the calculated

$\overset{o}{S}_\ell$ matrices defined as follows:

$$\sigma = \frac{1}{\ell_{max}} \sum_{0}^{\ell_{max}} |S_\ell - \overset{o}{S}_\ell| \cdot$$

Figure I exhibits the calculated potentials for each iteration and the respective values of χ^2 and σ. It is interesting to observe that though we started with a quite different potential from that which originated the input S-matrix, after seven interactions, the procedure returns back to the same original potential. This suggests that the linearization of Eq. (2.1) does not restrict in a substantial way the applications of the procedure.

3. THE DATA ANALYSIS

As data we used the measurements of elastic scattering cross sections for the $\alpha + {}^{12}C$ collision at E_{LAB} = 120 MeV, 145 MeV and 172,5 MeV of S. Wiktor et al. in the angular interval from $\theta_{cm} = 6°$ to $\theta_{cm} = 90°$, 70° and 60° respectively in investigating the actual shapes and uncertainties in the optical potential determination from the experimental data. Figure II shows their data as dots. The solid curve is one of our optica potential fits obtained by the inversion procedure previously described and will be explain in detail later. The insert in this figure is the classical deflection function obtained from the phase-shifts of the 145 MeV optical potential of reference (6). One should notice that the experimental data cover five orders of magnitude in the cross section with errors around 5% and extends beyond the classical rainbow angle ($\theta_{cm} \approx 50°$).

As our task is to exhibit not only the shape of the potential but also its uncertainties as determined by the data, we generated from the original data 15 new angular distributions by adding to them white noises with widths given by the experimental errors. The totality of 45 angular distributions, 15 for each energy value were the starting point of our analysis. As the experimental angular distributions contains around 40 to 50 points, insufficient to make phase shifts analysis, we enlarged the initial data set by including 50 new points for each angular distribution, determined from a cubic spline interpolation. These enlarged sets were used to search for the phase-shifts that best fit the data. In the search, we varied only those S_ℓ for $0 \le \ell \le 25$. The other S_ℓ values were taken from the optical potential of reference (6). Figure III summarizes the S_ℓ values found in our analysis. The vertical scale is $|S_\ell|$ and the horizontal scale the value of ℓ. The result is plotted as vertical bars centered on the mean value of $|S_\ell|$ and with widths equal to twice the RMS deviation from the mean value. We observe that the uncertanty in $|S_\ell|$ increases as ℓ decreases reflecting the relatively low sensitivity of the cross section to the low values of the angular momentum.

To each one of the 45 sets of S-matrix we applied the inversion procedure described in the previous section, using $\ell_{max} = 40$, $r_{max} = 10fm$ and a base of $N = 20$ linear splines. In all cases $\tilde{V}(r)$ was taken as the W-S potential given in the third column of table I. Figure IV exhibits our results. The 15 optical potentials found by the inversion procedure are plotted as small dots. The open circles (connected by the dashed line) correspond to the mean value of the potentials for each radial distance. The solid curve represents the W-S optical potential of reference (6). For each energy we observe that for $r \ge 3fm$, the surface region, the uncertainties in the potential are small and our results agree with the optical potential of reference (6) except for the 145 MeV case where the shape exhibits some structure outside the uncertainty bars. In the inner region ($r < 3fm$) the potentials deviates substantially from that of reference (6). In particular, not only does the imaginary potential exhibit very large negative values but also the real potential also becomes repulsive the lower the entrance channel energy. From our point of view, these effects in the inner region as a function of the energy can be qualitatively understood as resulting from the exclusion principle that inhibits the existence of $\alpha + {}^{12}C$ configuration in the ${}^{16}O$ system for lower values of the excitation energy. We should also point out the fact that the uncertainties in the potential get larger as the $\alpha + {}^{12}C$ approach one another. This basically reflects the uncertainties found in the determination of the S-matrix due to the centrifugal barrier since S_ℓ is more sensitive to the inner region for lower values of ℓ.

4. CONCLUSIONS

The application of the inversion procedure for the determination of the optical potential from the elastic S-matrix elements, first proposed by Mackintosh et al.[4] worked well for the $\alpha + {}^{12}C$ elastic scattering data at E_{LAB} = 120 MeV, 145 MeV and 172,5 Mev[8]. We found both the optical potentials for the entrance channel energies measured and also their uncertainties associated with the experimental errors. The uncertainties found agree with the general belief that the optical potential for ion collisions is not well determined in the inner region. Besides these main results we also found that as the energy decreases the imaginary part of the potential increases negatively and the real part becomes repulsive suggesting the existence of a hard core in the inner region for low entrance channel energies. We believe that this behavior is of a general character, reflecting the constraint imposed by the exclusion principle. If this is so, then we may expect that this effect is stronger for heavier ion collisions at the same entrance channel energy per nucleon.

ACKNOWLEDGMENTS

We would like to thank S. Wiktor for kindly providing us with the scattering cross sections for the $\alpha + {}^{12}C$ system.

TABLE I

Parameters	Pot. of Ref. 6	Initial potential
V_0	112.8MeV	80.MeV
r_0	0.673fm	0.773fm
a	0.82fm	0.50fm
W_0	16.8MeV	0.0
r_0^1	1.076fm	——
a_1	0.53fm	——

FIGURE CAPTIONS:

Figure I. Real and imaginary parts of the inversion potential after each iteration (dashed line) and the target potential of reference (6) (solid line).

Figure II. Experimental elastic angular distributions of α + ^{12}C at E_α = 172.5 MeV, 145 MeV and 120 MeV. The solid curve is one of our optical potential fits obtained by the inversion procedure. The insert is the classical deflection function obtained from the 145 MeV optical potential of reference (6).

Figure III. The solid bars represent the RMS deviation of $|S_\ell|$ obtained from the phase-shift analyses centered in the mean valve $|\bar{S}_\ell|$.

Figure IV. Optical potentials obtained by inversion (small dots). The open circles connected by the dashed-line correspond to the mean value of the potentials. The solid curves are the W-S optical potentials of reference (6) for each energy.

TABLE CAPTION

Table I. The first column gives the parameters, the second column their values as used in reference (5) for E_α = 172.5MeV and the third column the values of the parameters for the initial potential in the iterative procedure.

REFERENCES

1. U. Buck
   Rev.Mod.Phys. 46 (1974) 369.

2. R. Lipperheide, H. Fiedeldey
   Zeitschrift für Physik. A286 (1978) 45.

3. E. Kujawski
   Phys.Rev. C6 (1972) 709.

4. A.A. Ioannides and R.S. Mackintosh
   Nucl.Phys. A438 (1985) 354.

5. S.G. Cooper and R.S. Mackintosh
   Inversion problems (1989) pg. 707.

6. S. Wiktor, C. Mayer-Böricke, A. Kiss, M. Ragge, P. Turek, H. Dabrowski
   Acta Physica Polonica, nº 5 (1981) 491.

7. M. Abramowitz and I.A. Segun
   Handbook of Mathematical Functions, Dover Publications, Inc., New York

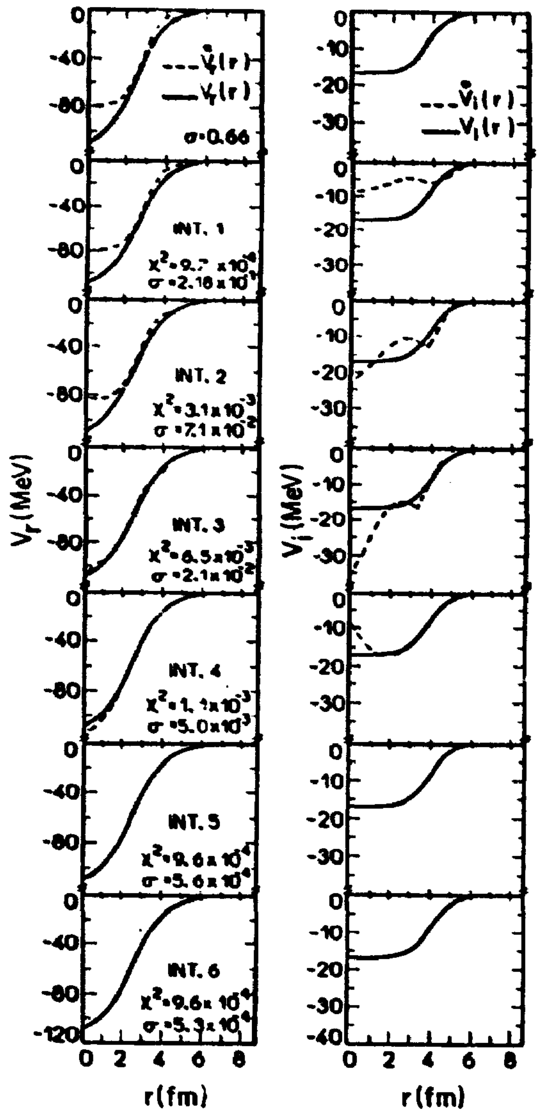

V_r (MeV)
V_i (MeV)
r (fm)
σ=0.66
INT. 1
INT. 2
INT. 3
INT. 4
INT. 5
INT. 6

FIG. I

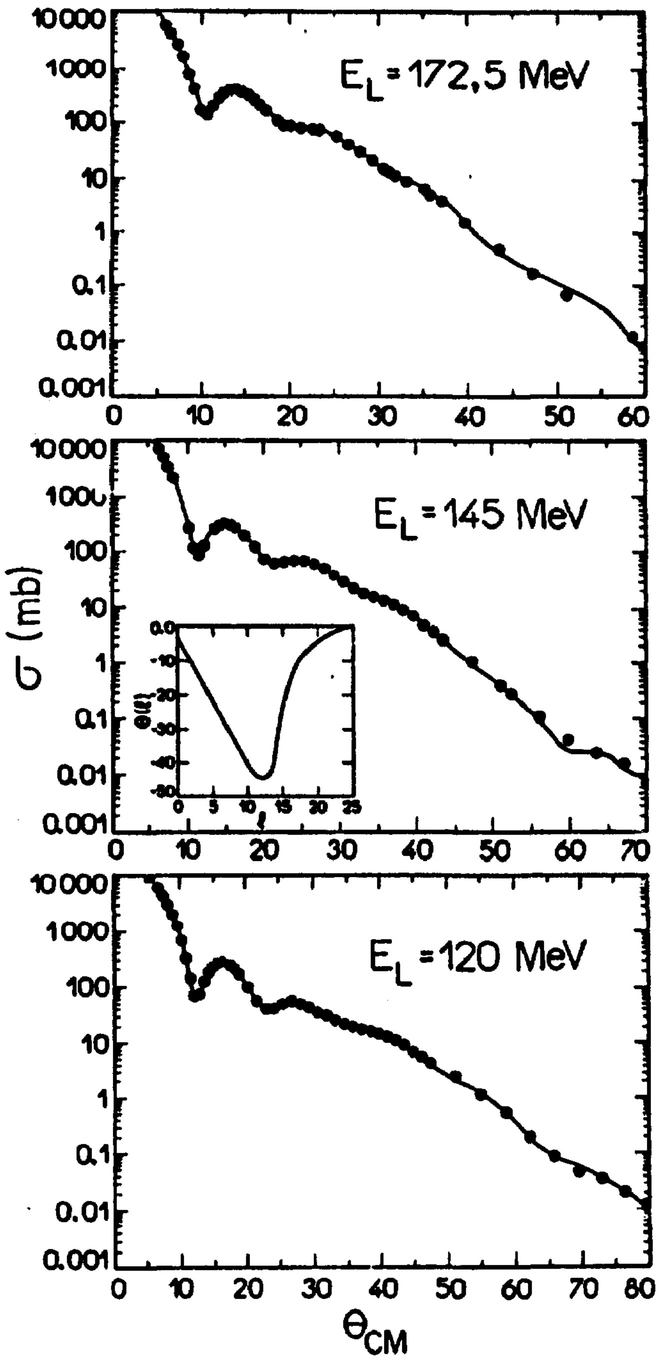

E_L = 172,5 MeV
E_L = 145 MeV
E_L = 120 MeV
σ (mb)
Θ_{CM}

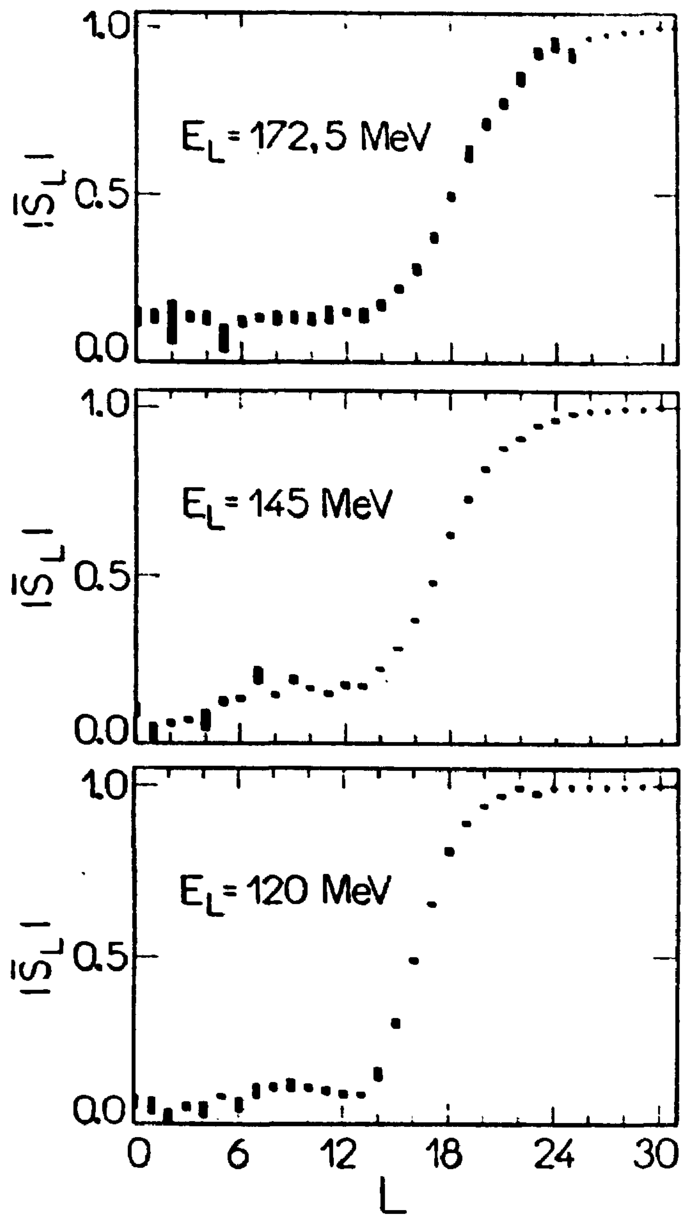

FIG. III

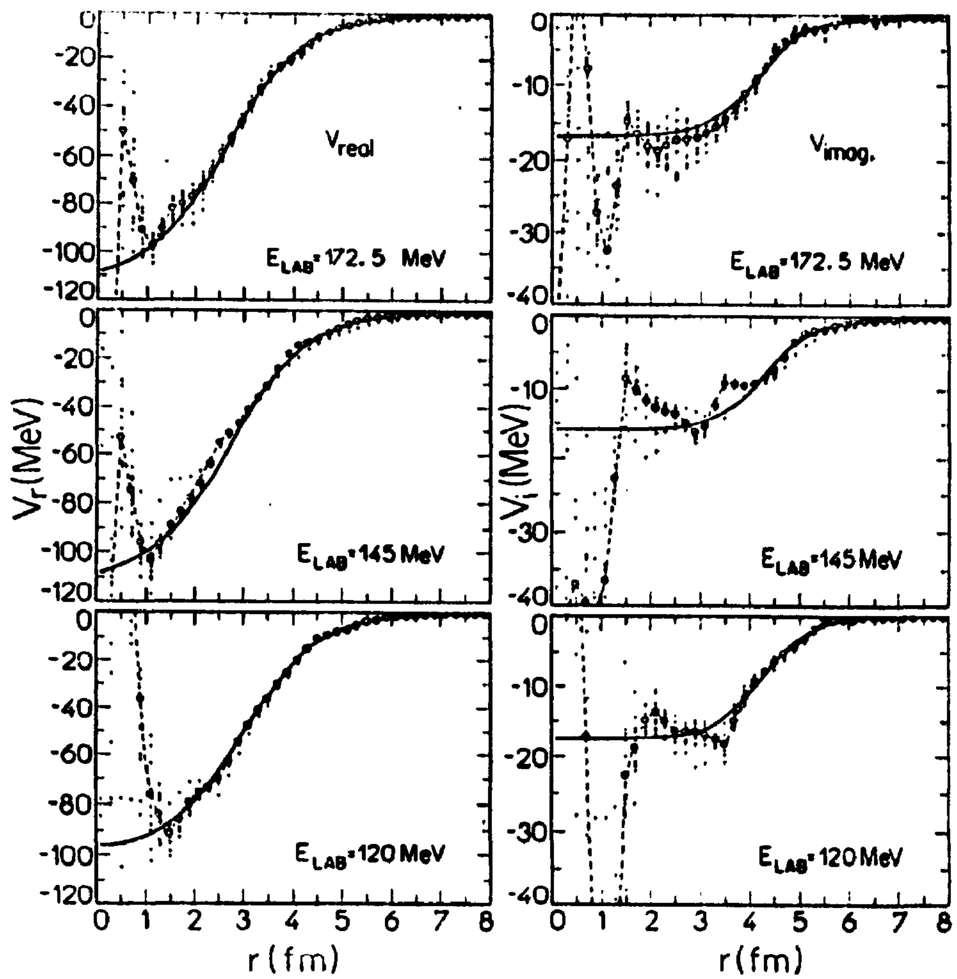

FIG. IV